Journal of Hazardous Materials 341 (2018) 304–312

Contents lists available at ScienceDirect

Journal of Hazardous Materials

journal homepage: www.elsevier.com/locate/jhazmat

Interplay between flow and bioturbation enhances metal efflux from low-permeability sediments

Minwei Xie[a,b,*], Ning Wang[a,c], Jean-François Gaillard[a], Aaron I. Packman[a]

[a] Department of Civil and Environmental Engineering, Northwestern University, 2145 Sheridan Road, Evanston, IL 60208-3109, USA
[b] Marine Envrionmental Laboratory, HKUST Shenzhen Research Institute, Shenzhen 518000, China
[c] Faculty of Geosciences and Environmental Engineering, Southwest Jiaotong University, Chengdu, Sichuan, 610031, China

HIGHLIGHTS

- Hydrodynamic force enhances efflux of dissolved Cu from low-permeability sediments.
- Interplay between flow and bioturbation further increases efflux of dissolved Cu.
- Bioturbation produces substantial physical and chemical heterogeneity in sediments.
- Bioturbation destabilizes sediments and facilitates sediment resuspension.

GRAPHICAL ABSTRACT

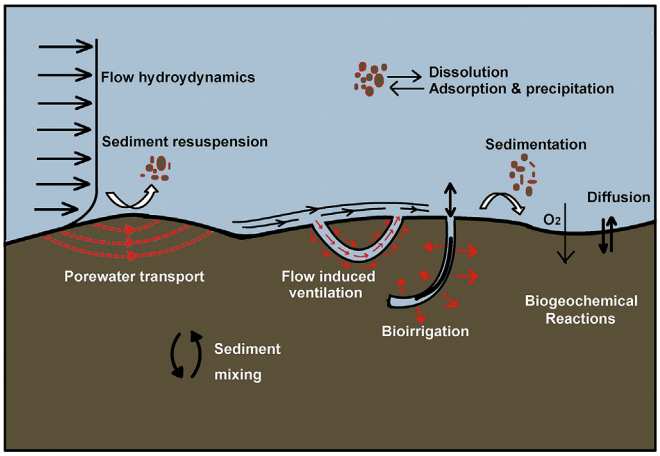

ARTICLE INFO

Article history:
Received 4 February 2017
Received in revised form 24 July 2017
Accepted 1 August 2017
Available online 2 August 2017

Keywords:
Contaminated sediments
Hydrodynamics
Bioturbation
Nereis virens
Metal efflux

ABSTRACT

Understanding the interplay effects between processes such as hydrodynamic forcing, sediment resuspension, and bioturbation is key to assessment of contaminated sediments. In the current study, effects of hydrodynamic forcing, sediment resuspension, and bioturbation by the marine polychaete *Nereis virens* were evaluated both independently and together in a six-month flume experiment. The results show that hydrodynamic forcing without resuspension or worm action slightly enhanced efflux of dissolved Cu to the water column, sediment resuspension released considerable amounts of dissolved Cu, and interactions between hydrodynamics and worm burrowing further enhanced Cu efflux. In non-bioturbated sediments, fine particles were only resuspended to the overlying water under the highest imposed shear stress, 0.58 Pa. However, bioturbated sediments were resuspended under all shear stresses tested (0.11–0.58 Pa), indicating that bioturbation destabilized the sediment bed. Further, increases in fluid shear following bioturbation caused rapid releases of dissolved Cu to the overlying water within a few hours. Cu efflux under fluid shears of 0.47 Pa and 0.58 Pa were 360× and 15× greater after the introduction of worms compared with the same flow conditions without their presence. Overall, our results

* Corresponding author at: Marine Environmental Laboratory, Shenzhen Research Institute, Hong Kong University of Science and Technology, Shenzhen 518000, China.
E-mail addresses: minwei.xie@gmail.com, minwei.xie@qq.com (M. Xie).

http://dx.doi.org/10.1016/j.jhazmat.2017.08.002
0304-3894/© 2017 Elsevier B.V. All rights reserved.

indicate that the release of metals from low-permeability sediments is greatly enhanced by interactions between flow and bioturbation.

© 2017 Elsevier B.V. All rights reserved.

1. Introduction

Metal contaminants in water bodies can accumulate and reside in sediments for a very long time. These metals are not permanently sequestered, but instead are dynamically partitioned between sediment particles, porewaters, and the overlying water column [1]. The fate of metals in sedimentary environments is regulated by a wide range of physical, chemical and biological processes [2]. Since the early 1980s, when environmental problems caused by contaminated sediments were widely recognized, considerable efforts have been made to remediate contaminated sites [3]. A comprehensive assessment of site contamination status and associated environmental risks is generally needed before remedial decisions are made. Development of a site-specific conceptual site model (CSM) is the first step to understand the fate and transport of contaminants while identifying the governing processes that control the mobility and bioavailability of contaminants is critical in constructing a CSM [3–5].

It is now recognized that sediments represent a highly complex system and that the fate of contaminants is highly dependent on an interrelated suite of sedimentary processes. Biogeochemical processes involving a series of electron acceptors (O_2, NO_3^-, MnO_x, Fe-$O(OH)_x$, SO_4^{2-}, *etc.*) redistribute metals between sediment particles and porewaters [6,7]. In low-permeability sediments ($k < 10^{-12}$ m^2), porewater transport is dominated by slow diffusive processes, leading to stratified biogeochemical zonation within the sediments [8,9]. The diffusion of metals across the sediment water interface (SWI) has been considered as the predominant pathway for release of metal ions to the water column in such low permeability sediments [10]. Interfacial advective fluxes of solutes are also known to be important in permeable sediments [11,12]. However, the effects of hydrodynamic forcing on efflux of metals from low-permeability sediments are frequently neglected in site assessments [2,13]. In estuarine environments, natural processes such as tidal cycles and wind induced waves generate variable hydrodynamic forcing over sediment bed across the whole estuary, with reported bottom shear stresses ranged from 0.05 to 1 Pa [14,15]. In our previous work, we also observed that increasing flow shear and sediment resuspension both enhanced the efflux of Cu from low-permeability sediments [13]. Bioturbation, including particle reworking and burrow ventilation, further complicates the system by introducing significant physical, chemical and biological heterogeneities [16–20]. Sediment reworking activities, such as construction and maintenance of burrows, greatly increase the area of the SWI [21]. But this burrow surface area should not be considered simply as an extension of the sediment surface as it contains strong chemical gradients and shows high temporal variabilities [21,22]. Ventilation of oxygenated water into burrows modifies redox and pH distributions in porewater surrounding the burrows, and enhances metal fluxes in sediments [23–25]. Because burrow formation induces such a wide change in sediment properties, we define bioturbation here as all activities of macrofauna that alter sediment pore structure and enhance motion and fluid motion through the sediments.

While the effects of hydrodynamic forcing and bioturbation on the fate and mobilization of metals have been individually studied, the interactions between these two processes have not been evaluated in detail. Therefore, to improve understanding of how the interplay of hydrodynamic forcing and bioturbation controls the mobility and efflux of Cu in low-permeability sediments, we conducted a long-term flume study to evaluate the release of Cu to porewater and overlying water under a range of hydrodynamic conditions with and without bioturbating organisms.

2. Material and methods

2.1. Experimental materials

Metal-contaminated sediments were obtained from Portsmouth Naval Shipyard (PNS). PNS is located on an island at the mouth of the Piscataqua River, Portsmouth Harbor, which is a tidal estuary located at the boundary of Maine and New Hampshire [26]. The water in vicinity of PNS has a salinity of 30 ~ 32‰. The site has a water depth of ~6 m and is subject to strong tidal influences, with a tidal range of 3 m [26]. The coastal sediments also provide habitat for a variety of organisms, including benthic fauna communities such as crustaceans, polychaete worms (Fig. 1b), clams, *etc.* [26]. It has been reported that *Nereis virens* [27], a typical marine polychaete, is an important local benthic species in Portsmouth Harbor, with a density of 117 individuals/m^2 [28]. Offshore sediments at this site have received substantial contamination from onshore construction and submarine repair activities. The sediments composed primarily of silt- and sand-sized particles and had a very low permeability. Cu and Zn were identified as the primary metal contaminants (Table S2). Approximately 100 L of contaminated sediments were collected in August 2013, transported in sealed buckets, and stored at 4 °C until experiments were performed.

To evaluate the interplay effects between flow and bioturbation on metals efflux, *N. virens* was introduced to the sediments as a model bioturbating organism. *N. virens* is classified in the functional group of gallery diffusers based on its feeding type, life habit and mobility, and reworks sediments primarily by excavating burrows [9,29]. *N. virens* was collected by Aquatic Research Organisms Inc. (ARO, NH) from Damariscotta River, Boothbay Harbor, which is a tidal estuary located close to the Portsmouth Harbor (~100 miles).

2.2. Flume setup and experimental procedures

Laboratory flumes have been widely used to study sediment transport and hyporheic exchange processes because they provide precise control of flow conditions [30,31]. The flume has a test section of 2.5 m long (x) × 0.2 m wide (y) × 1 m deep (z) (Fig. 1a). The sidewall of the flume is made of transparent acrylic, which allows direct visualization of the interior of the flume. An impermeable acrylic ramp was placed at the upstream end of the flume channel (x = 0 m) to ensure steady and uniform water flow over the sediment bed. A porous polyethylene sheet with 90–130 μm pores (Small Parts International) was emplaced vertically at the downstream end of the test section (x = 2.5 m) to retain the sediment bed without restricting porewater flow.

Before the experiments, the flume was cleaned with weakly acidified reverse osmosis (RO) purified water (pH = 2), run for 24 h, and then rinsed with purified RO water twice. 50 L of homogenized sediments were emplaced into the flume to form a 10-cm deep sed-

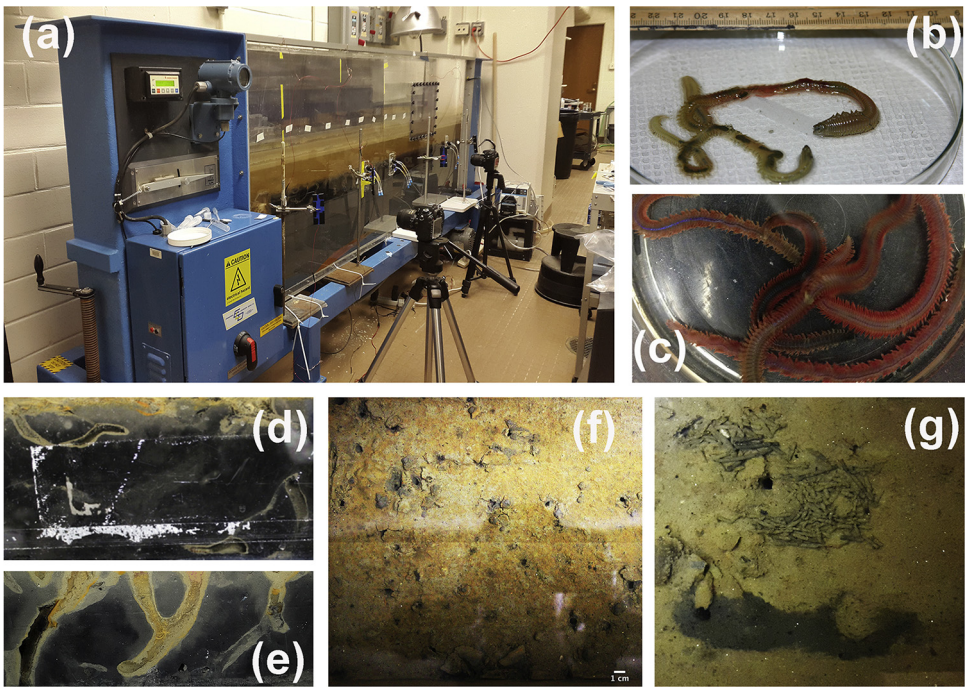

Fig. 1. Images of flume experiments. (a) Flume experimental setup. (b) Worms found in the PNS sediments. (c) *Nereis virens* used for the experiments. (d) (e) Side view of branched burrow networks. (f) Burrow openings at sediment surface. Scale bar = 1 cm. (g) Egested sediments deposited outside of burrows on the sediment surface.

iment bed. Two sets of rhizon *in situ* samplers (RISS) [32–34] with 0.15 μm pores (Sunvalley Solutions Inc., Florida) were installed through the flume sidewall during introduction of sediments to enable time-series porewater sampling. The two sets of RISS were installed in the test section at downstream distances $x = 0.9$ and 1.2 m. Each set included three RISS samplers inserted into the sediments at depths $d = 1$, 2, and 4 cm below the sediment bed surface. 180 L of artificial seawater (ASW) at a concentration of 32 g of sea salt (Tropic Marin, USA) per L of RO water, was carefully filled into the flume to yield a 15 cm overlying water column. The whole system was allowed to consolidate overnight, and then the recirculating water was drained and replaced with clean ASW on the second day to remove fines in water column before initiation of the experiments. The stream velocity profiles were recorded using a Micro Acoustic Doppler Velocimeter (MicroADV Lab, SonTek, CA) and the boundary shear stresses were calculated by fitting the measured velocities to the conventional logarithmic turbulent free-surface velocity profile (Fig. S1, Supporting information). To model bioturbation, 40 mixed-age adult *N. virens* were introduced into the sediment at week 19, yielding an average density of about 80 individuals/m^2 of sediment bed surface area, similar to the reported density of *N. virens* in the field [28]. To minimize evaporation during the experiment, the recirculating water was maintained at a constant temperature (20 °C) with a cooler and the flume was covered. To ensure that the experiment was conducted at a nearly constant volume over the entire period, the initial water level was labeled, and RO water was added every two days to compensate for the evaporation loss.

2.3. Experimental conditions

Experimental conditions were selected to span the important range of behavior found in the field, including varied levels of hydrodynamic shears, sediment resuspension, and bioturbation. Contaminated sediments were thus subject to varied overlying flow conditions with and without bioturbation. In previous studies with low-permeability sediments, we observed that increasing hydrodynamic forcing enhanced the release of dissolved Cu into the overlying water, and sediment resuspension caused large transitory perturbations in both dissolved and particulate Cu [13,35]. However, prior studies were limited to core-scale (10 cm diameter). Here, Cu efflux was observed under a range of flow conditions with and without bioturbation, including flow conditions that yielded resuspension of bed sediments. Four flow shear stresses (0.11, 0.22, 0.47, 0.58 Pa) were imposed over the sediment bed spanning the reported shear stress range in natural estuarine system [14,15]. The 0.11 Pa shear stress was used as the baseline shear. The overlying flow was fully turbulent at this condition, and kept the water column fully oxygenated throughout the experiments. Shear stresses of 0.22 and 0.47 Pa were still below the critical shear (CS) of the intact sediment bed and thus did not yield sediment resuspension. Sediment resuspension was achieved by increasing the flow shear to 0.58 Pa, which exceeded the CS of the sediment bed and scoured the surficial sediments. Due to the cohesive nature of the sediment bed, only a very limited amount of surficial sediments were scoured during sediment resuspensions (~1–2 mm, based on visual observation). For the first 4 weeks, the system was allowed to stabilize under baseline shear (0.11 Pa). Flow shear stresses were then varied in a stepwise fashion by altering the flow conditions between higher shear stresses and baseline shear stresses for periods of 1 week each (Fig. 2, Table S1, Supporting information). Finally, the highest shear (0.58 Pa) was imposed for 4 h to simulate a short-term resuspension event [13]. Cu concentrations were monitored throughout the entire period of these experiments to determine Cu efflux from the sediments.

Following the experiments on flow-induced Cu release without bioturbation, *N. virens* was introduced, and Cu efflux was determined again under all four shear stresses following bioturbation. The flume was returned to the baseline condition for 11 weeks to allow re-equilibration of sediments before introduction of *N. virens*. Forty *N. virens* were then introduced in week 19 (day 134), and the overlying water flow was kept at the 0.11 Pa baseline shear for 2 weeks to characterize the effects of bioturbation on Cu release under this flow condition. The flow was then varied in the same

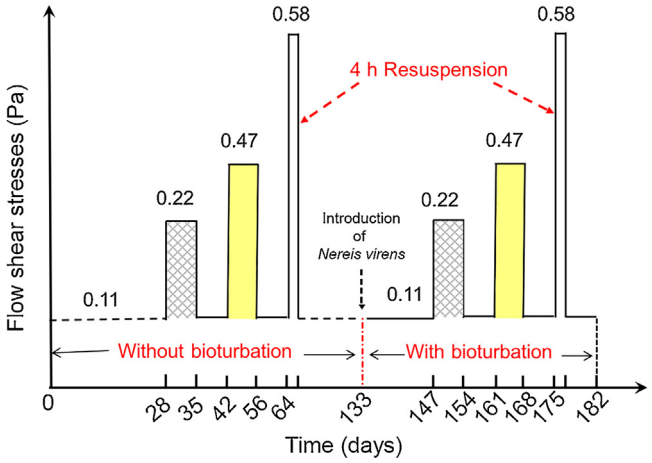

Fig. 2. Experimental conditions. Sediments were subject to four levels of flow shear (0.11, 0.22. 0.47, and 0.58 Pa) with and without bioturbation.

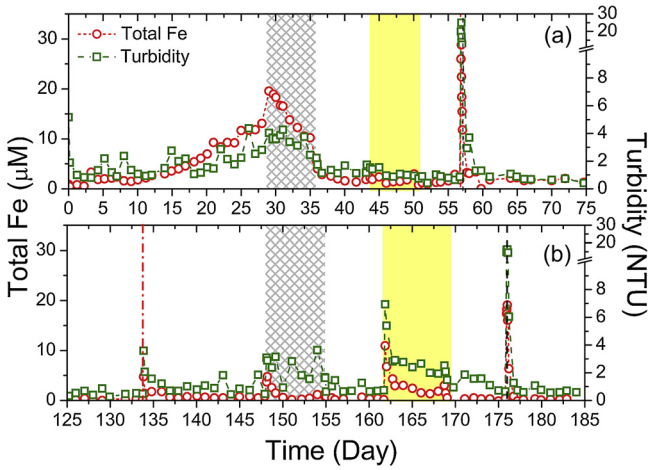

Fig. 3. Total Fe concentrations and turbidity in the overlying water under varying flow shear with and without bioturbation. Unshaded areas of the graphs indicate periods with baseline shear conditions (0.11 Pa). Cross-hatching and shading indicate periods with shear stresses of 0.22 Pa and 0.47 Pa, respectively. Black vertical dashed lines in day 57 (a) and day 176 (b) represent 4-h resuspension events. Red vertical dashed line on day 134 (b) represents introduction of 40 *N. virens*. (For interpretation of the references to color in this figure legend, the reader is referred to the web version of this article.)

sequence described previously to study the interactions between bioturbation and flow hydrodynamics. The overall experimental timeline is shown in Fig. 2.

2.4. Sampling and analysis

Dissolved oxygen (DO) was measured directly within the downstream end-well with a DO probe (HQ10, Hach). Overlying water samples were acquired daily for measurement of pH, turbidity, conductivity and dissolved and total metal concentrations. 24 mL of overlying water was collected daily and split into three 8 mL aliquots for analysis. One aliquot was used for measurement of pH (420Aplus, Thermo Orion), conductivity (Oakton Instruments) and turbidity (2100Q, Hach), and then returned to the flume following analysis. The other two aliquots were stored for measurements of dissolved and total metal concentrations. Following sample acquisition, 16 mL of clean ASW was added to the flume to maintain a constant volume of recirculating water. Samples for dissolved metals were filtered through a 0.2 μm filter and acidified with HNO_3 (trace metal grade, Sigma Aldrich) to pH < 2. Samples for total metals were acidified to pH < 2 without filtration. All water samples were stored at 4 °C before analysis. Cu concentrations in the water samples were analyzed by Zeeman Graphite Furnace Atomic Absorption Spectrometry (SpectrAA-800, Varian) [13]. Fe concentrations in the water samples were analyzed using the ferrozine colorimetric method (Supporting information) [36,37].

Porewater was sampled periodically – at least once per week for experiments performed without bioturbation and every 3–5 days in presence of *N. virens*– by RISS to characterize spatial and temporal patterns in dissolved Cu concentrations. The first 0.5 mL of porewater obtained from each RISS was discarded and another 2 mL of water was collected, acidified to pH < 2, and stored for metal analysis using the methods described previously.

3. Results

3.1. Particle dynamics and total Fe concentrations in the overlying water with and without N. virens

Fine particle transport was characterized by turbidity and total Fe concentrations in the overlying water (Fig. 3). Over the first 4 weeks (0.11 Pa baseline shear), total Fe concentrations in the overlying water remained unchanged for the first 10 days and then gradually increased at a rate of 0.645 μM/day ($r = 0.96$, $p < 0.001$). When the flow was increased to a shear stress of 0.22 Pa on day 29, total Fe abruptly increased from 13.1 to 19.6 μM and then gradually decreased at a rate of 1.90 μM/day ($r = 0.97$, $p < 0.001$). Overlying water turbidity showed similar trends – slightly increasing during the first 4 weeks under baseline shear condition (0.11 Pa), but decreasing under a constant shear of 0.22 Pa (Fig. 3a). Dissolved Fe concentrations in the overlying water remained below the detection limit at all times, and thus all Fe detected in the overlying water was particulate. The decrease of both overlying water Fe concentrations and turbidity under the constant imposed shear of 0.22 Pa reflected net removal of particles from the overlying water following the initial increase in shear stress. Turbidity and Fe concentrations decreased to very low levels at the end of the period with 0.22 Pa. These concentrations remained very low even when the shear was increased to 0.47 Pa on day 43 (Fig. 3a), indicating that the redeposited particles were immobilized such that they were not re-entrained under higher hydrodynamic forcing. Increasing the bed shear to 0.58 Pa (above the critical shear) on day 57 yielded resuspension and caused a transient increase in particle concentrations in the overlying water. Particle concentrations rapidly decreased to the pre-resuspension level following reduction of the shear to 0.11 Pa.

To investigate the impact of the presence of worms, 40 *N. virens* were introduced into the sediment on day 134. The worms burrowed into the sediment within 1 h after they were introduced, and formed more than 100 burrows within 24 h of introduction. New burrows continued to be formed for ~10 days, yielding ~160 burrow openings at steady state (Fig. S3, Supporting information) and intermittent presence of *N. virens* in the burrows close to the flume side wall was observed throughout the experiment. Note that the number of burrow openings was 3–4 times greater than the number of worms, reflecting that *N. virens* produces highly branched burrows. Worm burrow openings ultimately comprised 0.5% ± 0.2% of the surface area (Fig. S3, Supporting information). This represented a substantial biological perforation of the sediment, as it yielded substantial macroporosity both at the SWI and within the bed (Fig. 1d–f). The worms also created mound structures around burrow openings by egesting sediment particles at the sediment surface (Fig. 1f, g). These sediment-reworking activities caused a temporary remobilization of particles to the overlying water, yielding small increases in total Fe and turbidity after intro-

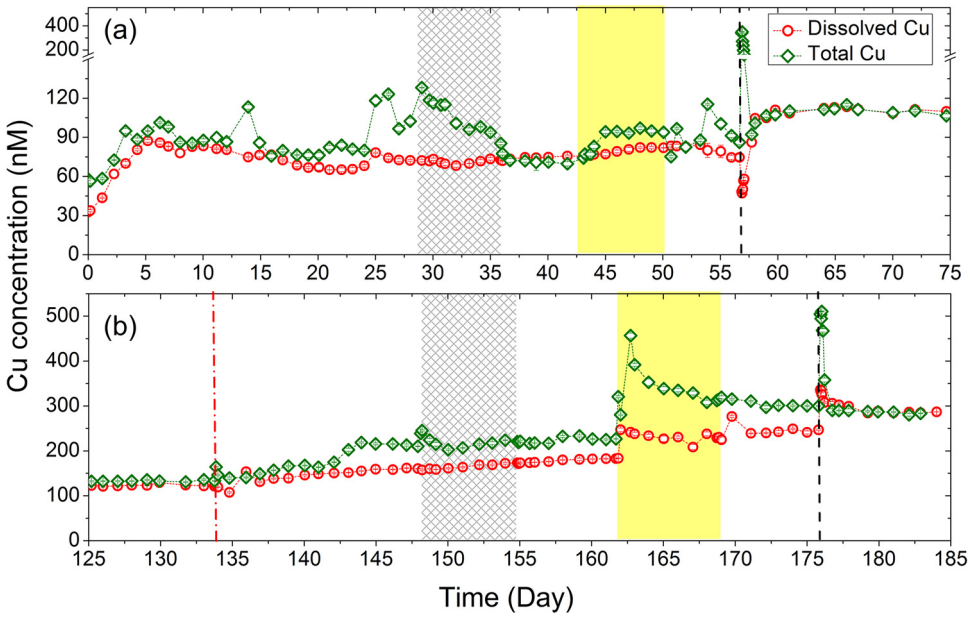

Fig. 4. Dissolved and total Cu concentrations in overlying water (a) without bioturbation, and (b) with bioturbation.

duction of worms, which then decreased back to the original levels (before worm introduction) within two days (Fig. 3b). When flow shear was increased to 0.22 Pa on day 148, total Fe concentrations and turbidity increased slightly. Fe concentrations then decreased within two days while the turbidity fluctuated for the entire week. When flow shear decreased to 0.11 Pa on day 155, the turbidity returned to baseline levels. Increasing the flow shear to 0.47 Pa on day 162 greatly increased total Fe and turbidity, both of which then slowly decreased over the following week of constant flow. The four-hour sediment resuspension (0.58 Pa) on day 176 caused an abrupt and highly transitory increase in both total Fe and turbidity, which decreased back to the pre-resuspension level when resuspension ceased.

3.2. Cu concentrations in the overlying water

Release of both dissolved Cu ($[Cu]_d$) and total Cu ($[Cu]_t$) to the overlying water was strongly controlled by hydrodynamics and bioturbation, and particularly by the interactions between the two processes (Fig. 4). For the first 5 days under the 0.11 Pa baseline shear, both $[Cu]_d$ and $[Cu]_t$ were gradually released to the overlying water at rates of 11.0 nM/day ($r = 0.99$, $p < 0.001$) and 8.28 nM/day ($r = 0.94$, $p = 0.002$), respectively (Fig. 4a). From day 5 to day 28, $[Cu]_d$ then decreased slightly at a rate of 0.739 nM/day ($r = 0.76$, $p < 0.001$) while $[Cu]_t$ remained approximately constant ($p = 0.59$). When flow shear was increased to 0.22 Pa on day 29, $[Cu]_d$ first decreased and then increased (Fig. 4a) while $[Cu]_t$ continuously decreased. Following the decrease in flow shear from 0.22 to 0.11 Pa on day 36, $[Cu]_t$ decreased to about the same level as $[Cu]_d$, indicating complete removal of particulate Cu ($[Cu]_p = [Cu]_t - [Cu]_d$) (Fig. 4a). When flow shear was increased to 0.47 Pa on day 43, both $[Cu]_d$ and $[Cu]_t$ increased (Fig. 4a). The increase in $[Cu]_d$ when flow shear was increased from 0.11 to 0.22 Pa and again from 0.11 to 0.47 Pa suggests that increasing hydrodynamic forces on the bed surface promoted the efflux of dissolved Cu to the overlying water. On day 57, increasing shear to 0.58 Pa for 4 h caused sediment resuspension with an abrupt but highly transitory increase in $[Cu]_t$. Following the cessation of sediment transport, $[Cu]_t$ rapidly decreased (within one day) to pre-resuspension levels. However, sediment resuspension induced different effects on dissolved Cu. When sediment resuspension was initiated, $[Cu]_d$ first decreased by 30 nM within 1 h and then increased for the following 28 h, resulting in a net elevation of $[Cu]_d$ in the overlying water by ~30 nM (Fig. 4a).

After introduction of *N. virens* on day 134, both $[Cu]_d$ and $[Cu]_t$ gradually increased at rates of 2.98 nM/day ($r = 0.88$, $p < 0.001$) and 6.06 nM/day ($r = 0.92$, $p < 0.001$) (Fig. 4-5b). When flow shear was increased to 0.22 Pa on day 148, $[Cu]_t$ immediately increased from 210 nM to 245 nM and then gradually decreased to 221 nM over the following week. $[Cu]_d$ gradually increased under this flow condition (0.22 Pa) at a rate of 2.48 nM/day ($r = 0.99$, $p < 0.001$). Following the reduction of flow shear to 0.11 Pa on day 155, both $[Cu]_d$ and $[Cu]_t$ continued to increase but at lower rates, 1.71 nM/day ($r = 0.97$, $p < 0.001$) for $[Cu]_d$ and 1.58 nM/day ($r = 0.64$, $p = 0.05$) for $[Cu]$. Increasing the flow shear to 0.47 Pa on day 162 led to rapid release of Cu to the overlying water: $[Cu]_d$ rapidly increased from 183 to 247 nM, and $[Cu]_t$ from 226 to 457 nM within 4 h. Both $[Cu]_d$ and $[Cu]_t$ then gradually decreased to 230 nM and 315 nM, respectively, over the following week. The 4-h resuspension (0.58 Pa) on day 176 also led to a rapid release of Cu: following initiation of the sediment resuspension on day 176, $[Cu]_d$ and $[Cu]_t$ rapidly increased from 247 to 336 nM, and 300 to 505 nM, respectively, within 0.5 h. After resuspension ceased, both $[Cu]_d$ and $[Cu]_t$ then decreased to 306 and 290 nM. The resuspension event resulted in a net increase in $[Cu]_d$ by ~60 nM.

3.3. Temporal evolution of Cu concentrations in porewater

Dissolved Cu concentrations in porewater ($[Cu]_{pw}$) collected from RISS located at $x = 0.9$ and 1.2 m showed consistent spatial trends without bioturbation, but exhibited greater spatial and temporal variability after *N. virens* was introduced. Cu concentrations in porewater collected at $x = 1.2$ m are shown in Fig. 5. Cu concentrations in porewater collected at $x = 0.9$ m are shown in Fig. S4, Supporting information. Before introduction of the worms on day 134, Cu concentrations in porewater at $d = 1$ cm were significantly greater than the Cu concentrations both in overlying water ($p < 0.005$) and at $d > 1$ cm ($p < 0.001$) (Fig. 5a, Table S3, Supporting

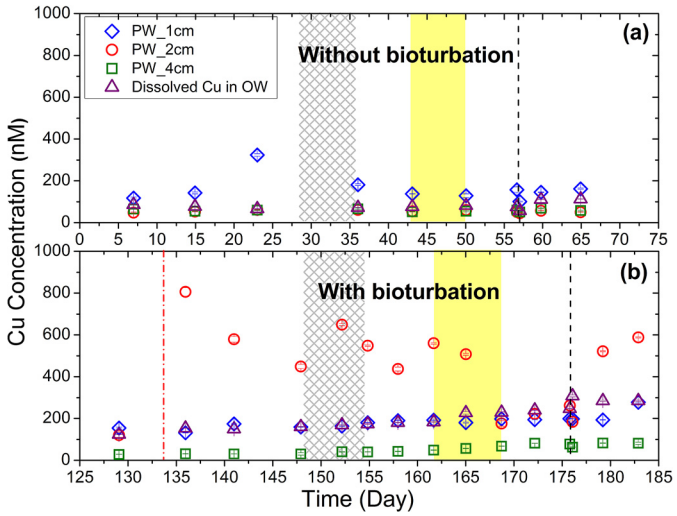

Fig. 5. Temporal variations of Cu concentrations in porewater observed by RISS emplaced at different depths (a) Without bioturbation, (b) With bioturbation. Porewater samples were collected from RISS located at $x = 1.2$ m.

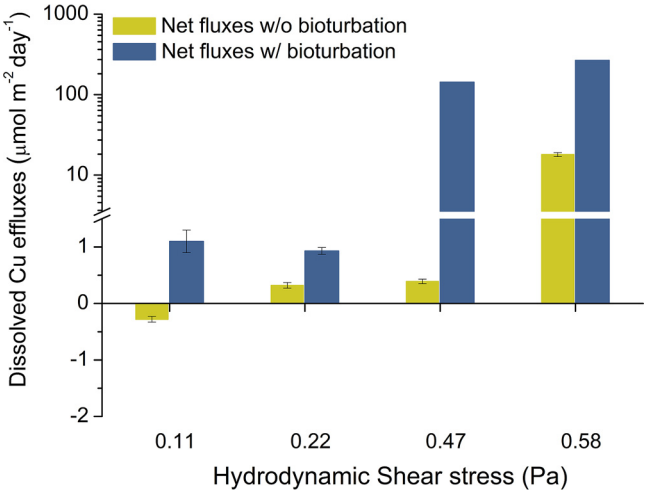

Fig. 6. Efflux of dissolved Cu from sediments under different hydrodynamic shear stresses with and without bioturbation.

information), suggesting that surficial porewater was a source of Cu to the overlying water. After introduction of worms to the sediment on day 134, Cu concentrations in porewater at $d = 2$ cm substantially increased and became significantly higher than Cu concentrations in porewaters at other depths ($d = 1$ and 4 cm) ($p < 0.001$) and in overlying water ($p < 0.005$) (Fig. 5b, Table S4, Supporting information).

Vertical profiles of porewater Cu concentrations were similar between the two measurement locations ($x = 0.9$ and 1.2 m) under all flow conditions before introduction of *N. virens* ($p > 0.05$, Table S7, Supporting information). However, after the introduction of *N. virens*, the porewater Cu concentrations at all depths collected at the two locations became significantly different ($p < 0.001$) (Table S8). Cu concentrations in porewater at $d = 4$ cm, $x = 0.9$ m significantly increased at a rate of 3.93 nM/day ($r = 0.84$, $p < 0.001$) (Fig. S4b) and gradually exceeded Cu concentrations in porewaters at other depths ($p < 0.001$) (Table S6, Supporting information).

3.4. Efflux of Cu to the water column

Net Cu efflux from the bed was calculated in terms of the overall mass balance of dissolved Cu in the overlying water. The net flux of dissolved Cu across the SWI was obtained by normalizing the rate of change in the overlying water dissolved Cu concentration with the volume of overlying water and SWI area, as detailed in the Supporting information. To investigate how the interplay between flow and bioturbation affects Cu efflux from low-permeability sediments, we compared results between the first half of experiment without *N. virens* and the second half of the experiment with *N. virens*. Though dissolved Cu concentrations in the overlying water became substantially elevated, the total mass of Cu in the overlying water was minimal compared to the Cu accumulated in the sediments. Before the introduction of *N. virens*, increasing flow shear from 0.11 to 0.47 Pa slightly increased the net Cu efflux from −0.28 to 0.39 $\mu mol\ m^{-2}\ day^{-1}$ (Fig. 6). Resuspension under the highest shear, 0.58 Pa, significantly increased the net Cu efflux ($p < 0.001$, Table S9). After *N. virens* was introduced on day 134, the net Cu efflux under each flow condition was all substantially higher than the corresponding Cu efflux without bioturbation, indicating that interactions between bioturbation and flow further enhanced Cu efflux from the sediments relative to the effects of flow alone.

4. Discussion

4.1. Effects of bioturbation on dissolved Cu in porewater

Our previous studies showed that oxidation of surficial sediments liberates aqueous metals into surficial porewater, which facilitates the efflux of metals to the overlying water column [13,35]. Here, we observed that Cu concentrations at 1 cm porewater were consistently higher than those measured in the overlying water and in porewater at depth >1 cm without bioturbation (Figs. 5 and S4), indicating that surficial sediments were a source of Cu to the overlying water.

Following introduction of *N. virens*, dissolved Cu concentrations in porewater showed both temporal and spatial variations. Dissolved Cu in porewater at $d = 2$ cm, $x = 1.2$ m increased right after the introduction of *N. virens* and varied for the remainder course of the experiment, while dissolved Cu in porewater at $d = 4$ cm, $x = 0.9$ m gradually increased (Fig. 5b, Fig. S4b, Supporting information). However, these effects were not observed at other locations, indicating spatial heterogeneity in porewater chemistry induced by *N. virens* burrowing. *N. virens* constructed multi-branched burrow networks in sediments when introduced into the sediments, yielding substantial macroporosity both at the SWI and in the bed [21,27,38]. This is consistent with the general behavior of *N. virens* observed in the field: *N. virens* creates semi-permanent U-shaped and branched burrows [21], with two major phases of burrow construction–digging and consolidation of galleries for five to seven days, followed by a maintenance phase with intermittent burrowing primarily within existing burrows [39,40]. While excavating for burrows, *N. virens* also ventilates the burrows by intermittently irrigating oxygenated overlying water at a rate of ~0.14 L day^{-1} per organism [9,23,27]. Subsequently, oxidation of anoxic sediments adjacent to the burrows may occur, resulting in localized mobilization of metals in sediments close to burrows [41]. Therefore, it is likely that the RISS located at $d = 2$ cm, $x = 1.2$ m, and at $d = 4$ cm, $x = 0.9$ m collected porewater directly from or indirectly influenced by oxic worm burrows, while RISSs at other sampling locations remained in undisturbed sediments and thus were not affected by bioturbation.

4.2. Interplay effects between flow and bioturbation on mobilization and efflux of dissolved Cu

Previous study showed that hydrodynamic forcing plays a critical role in mobilizing metals from surficial sediments with permeability as low as 10^{-15} m^2. Here before the introduction of *N. virens*, we also observed that release of dissolved Cu from the sediment increased with hydrodynamic shear on the bed surface (Fig. 6). When *N.virens* was present, the interactions between flow and bioturbation further enhanced the efflux of dissolved Cu. Following bioturbation dissolved Cu concentrations in the overlying water increased at rates of 2–3 nM/day under shears of 0.11 and 0.22 Pa. However, dissolved Cu efflux was much more rapid when shear was increased to 0.47 Pa and further to 0.58 Pa (386 and 761 nM/day, respectively) (Fig. 4b). Similarly, the overall Cu efflux from the bed was two orders of magnitude greater under the higher-shear conditions of 0.47 and 0.58 Pa than under the lower-shear conditions of 0.11 and 0.22 Pa (Cu efflux = 1.1, 0.93, 143 and 267 μmol m^{-2} day^{-1} under shears of 0.11, 0.22, 0.47, and 0.58 Pa, respectively) (Fig. 6).

Overall, these results clearly show that bioturbation enhanced flow-induced efflux of Cu from the sediments relative to the effects of flow alone. In non-bioturbated fine sediments, low permeability limits exchange across the sediment-water interface [8], restricting fluxes to slow, near-diffusive levels [42]. Hydrodynamic forcing can enhance solute exchange by sharpening solute concentrations gradients, by periodic turbulent disruptions in the diffusive boundary layer, and/or by flushing of the uppermost sediments [43]. The enhanced solute exchange at the SWI led to deeper penetration of DO under higher flow shear stresses (Fig. S5a), which in turn may facilitate the oxidation of anoxic surface sediments. In bioturbated sediments, burrow structures provide macroporosity and increase the connectivity between overlying water and porewater. Bioturbation also leads to localized mobilization of metals adjacent to the burrow where oxidation of anoxic sediments occur, creating microniches in sediment porewaters with elevated levels of dissolved metals [41]. When flow is imposed over the bioturbated sediments, preferential flow through the subsurface macropores may occur, resulting in passive ventilation of the burrows [44,45]. Though comprised only a small proportion of the bulk volume of sediment, subsurface macropores can significantly enhance the preferential advective exchange at the SWI [46], and the rapid turnover of water in these macropores is likely to introduce variabilities in porewater solute concentrations under varied flow conditions (Fig. 5b). Flow-burrow interactions have been shown to enhance surface-porewater exchange by a factor of at least 100 [47]. Further, this type of passive, flow-induced flushing of burrows increases with overlying flow rate and shear on the bed surface [30]. Therefore, we attribute the observed two-order-of-magnitude increase in Cu efflux under high flow in bioturbated sediments to enhanced hydrodynamic exchange through *N. virens* burrows.

4.3. Effects of flow and bioturbation on sediment transport

In cohesive sediments, such as the PNS sediments we used here, the stability of the sediment bed is regulated by competition between hydrodynamic forces that mobilize particles and attractive forces between particle grains [48]. Remobilization of sediment particles occurs when flow shear exceeds the critical shear stress [49,50]. Here, we found that in non-bioturbated sediments, remobilization of sediment particles occurred at the highest flow shear (0.58 Pa, above the critical shear of the consolidated bed) but not at lower shear stresses (0.11, 0.22, and 0.47 Pa) (Fig. 3a). Due to the cohesive nature of the sediment bed, only very limited amount of surficial sediments were scoured. These suspended particles were not removed from the system, but instead redeposit back to the sediment bed when resuspension ceased. Therefore, the perturbation of surface sediment structure was considered marginal. In contrast, following the introduction of *N. virens*, the bed sediments were mobilized under all flow conditions (0.11–0.58 Pa) (Fig. 3b). This enhanced sediment mobility indicates that bioturbation substantially lowered the critical shear for resuspension and thus destabilized the sediment bed. Prior studies have found that benthic organisms can both stabilize and destabilize sediment beds [51–53]. Most burrowing macrofauna have been found to destabilize sediments through burrowing and feeding activities, increasing bed roughness, and deposition of more-erodible fecal pellets at the sediment surface [51,54–56]. Here, *N. virens* was observed to excavate burrows, eject sediment particles onto the bed surface, and increase bed roughness. All of these outcomes contribute to destabilizing bed sediments and enhancing sediment resuspension.

4.4. Implications for assessment of contaminated sites

Results from the type of laboratory flume macrocosm used here are known to be readily transferrable to the field. Effective diffusion coefficient scaling relationships have been used in a variety of large-scale laboratory studies and field applications to compare benthic solute fluxes under a range of transport conditions (molecular diffusion, bioturbation, advection, shear, bed mobility and turbulence) [30,57]. Dynamics of fine particles observed in the present study – rapid entrainment of particles when flow shear exceeds sediment critical shear stress and removal of resuspended particles under base flow conditions – are also frequently reported in field experiments [58,59]. The results therefore provide information that can be used to improve understanding of contaminant dynamics at field sites.

The present study clearly showed that hydrodynamics and the presence of *N. virens* substantially enhance the efflux of Cu to the overlying water, but the exact mechanisms controlling interactions between flow, bioturbation, biogeochemistry and the associated mobilization of metals from the sediments remain undetermined, particularly with regard to the physiology of different bioturbators. *N. virens* has long been known as burrow-building bioturbator in coastal sediments, and creates galleries composed of structured burrows consolidated by a fine layer of organic mucus [39,40]. The bioirrigation of oxygenated water into burrows also modifies the redox condition in the burrow wall sediments. It still remains unresolved how these behaviors of *N. virens* changes the fine-scale redistribution of metals in sediments and how hydrodynamics influence these processes. Here we observed that flow interactions with burrow formation enhanced the bulk efflux of metals from the sediments. We also observed intermittent motion of *N. virens* within burrows, but we were not able to resolve the *in situ* response of metals at the spatial and temporal scales of *N. virens* motion. Microbial decomposition and associated remineralization of metals accumulated in dead organisms may also influence the mobility of metals [60]. Future studies should consider these processes and determine their contribution to the overall metal efflux to the water column in order to inform better understanding of the basic processes that control the fate of metals in sedimentary systems.

5. Conclusions

Determining fluxes of metals across the SWI is a central step in assessing contaminant mobility and the associated environmental risks. Identifying the governing processes that affect contaminant efflux and effects are critical to reduce the uncertainty in risk-based remedial decisions. While the effects of many important physical, chemical, and biological processes have been recently identified,

it is not well understood how these processes work together to control the fate and transport of contaminated sediments. Effects of hydrodynamic forcing on contaminant mobility in fine, cohesive sediments are frequently neglected. The results presented here not only show that hydrodynamic forcing facilitates the efflux of Cu from low permeability sediments, but also clearly indicate that interactions between flow and bioturbation substantially enhance the net efflux of dissolved Cu. These results indicate that interactions between time-variable flow, sediment resuspension, and bioturbation should be considered as potential governing processes in conceptual site models.

Acknowledgements

This research was supported by the Strategic Environmental Research and Development Program (ER-1745) and the National Science Foundation (EAR-1215898). We thank three anonymous reviewers for comments that help us improve the quality of the manuscript.

Appendix A. Supplementary data

Supplementary data associated with this article can be found, in the online version, at http://dx.doi.org/10.1016/j.jhazmat.2017.08.002.

References

[1] B. French, A. Turner, Mobilization, adsorption, and bioavailability of Pt and Pd in coastal sediments: the role of the polychaete, Arenicola marina, Environ. Sci. Technol. 42 (2008) 3543–3549.
[2] G.A. Burton, Metal bioavailability and toxicity in sediments, Crit. Rev. Environ. Sci. Technol. 40 (2010) 852–907.
[3] USEPA, National Sediment Quality Survey, The Incidence and Severity of Sediment Contamination in Surface Waters of the United States, USEPA, Washington, D.C, 1997.
[4] T. Sorell, K. McEvoy, Incorporating bioavailability considerations into the evaluation of contaminated sediment sites, Remediat. J. 23 (2013) 63–72.
[5] P. Adriaens, S. Bentley, F. Bohlen, T. Bridges, J. Davis, T. Dekker, R. Dickhut, N. Fisher, K. Gardner, A. Leeson, SERDP and ESTCP Expert Panel Workshop on Research and Development Needs for the In Situ Management of Contaminated Sediments, DTIC Document, 2004.
[6] P. Van Cappellen, J.-F. Gaillard, Biogeochemical dynamics in aquatic sediments, Rev. Mineral. Geochem. 34 (1996) 335–376.
[7] J.-F. Gaillard, H. Pauwels, G. Michard, Chemical diagenesis in coastal marine-sediments, Oceanol. Acta 12 (1989) 175–187.
[8] M. Huettel, I.T. Webster, Porewater flow in permeable sediments, in: The Benthic Boundary Layer: Transport Processes and Biogeochemistry, Oxford University Press, New York, 2001, pp. 144–179.
[9] E. Kristensen, Organic matter diagenesis at the oxic/anoxic interface in coastal marine sediments, with emphasis on the role of burrowing animals, Hydrobiologia 426 (2000) 1–24.
[10] A. Lerman, D. Imboden, J. Gat, Physics and Chemistry of Lakes, Springer, Berlin, 1995.
[11] M. Huettel, W. Ziebis, S. Forster, G.W. Luther Iii, Advective transport affecting metal and nutrient distributions and interfacial fluxes in permeable sediments, Geochim. Cosmochim. Acta 62 (1998) 613–631.
[12] C.E. Reimers, H.A. Stecher, G.L. Taghon, C.M. Fuller, M. Huettel, A. Rusch, N. Ryckelynck, C. Wild, In situ measurements of advective solute transport in permeable shelf sands, Cont. Shelf Res. 24 (2004) 183–201.
[13] M. Xie, N. Wang, J.-F. Gaillard, A.I. Packman, Hydrodynamic forcing mobilizes Cu in low-permeability estuarine sediments, Environ. Sci. Technol. 50 (2016) 4615–4623.
[14] R. Verney, J.-C. Brun-Cottan, R. Lafite, J. Deloffre, J. Taylor, Tidally-induced shear stress variability above intertidal mudflats in the macrotidal Seine Estuary, Estuar. Coasts 29 (2006) 653–664.
[15] R. Verney, J. Deloffre, J.-C. Brun-Cottan, R. Lafite, The effect of wave-induced turbulence on intertidal mudflats: impact of boat traffic and wind, Cont. Shelf Res. 27 (2007) 594–612.
[16] W. Ziebis, S. Forster, M. Huettel, B.B. Jørgensen, Complex burrows of the mud shrimp Callianassa truncata and their geochemical impact in the sea bed, Nature 382 (1996) 619–622.
[17] S. Papaspyrou, T. Gregersen, R.P. Cox, M. Thessalou-Legaki, E. Kristensen, Sediment properties and bacterial community in burrows of the ghost shrimp Pestarella tyrrhena (Decapoda: Thalassinidea), Aquat. Microb. Ecol. 38 (2005) 181–190.
[18] M.E. Hines, W.H. Orem, W.B. Lyons, G.E. Jones, Microbial activity and bioturbation-induced oscillations in pore water chemistry of estuarine sediments in spring, Nature 299 (1982) 433–435.
[19] R.C. Aller, Bioturbation and remineralization of sedimentary organic matter: effects of redox oscillation, Chem. Geol. 114 (1994) 331–345.
[20] K.R. Roche, A.F. Aubeneau, M. Xie, T. Aquino, D. Bolster, A.I. Packman, An integrated experimental and modeling approach to predict sediment mixing from benthic burrowing behavior, Environ. Sci. Technol. 50 (2016) 10047–10054.
[21] S. Widdicombe, H. Needham, Impact of CO2-induced seawater acidification on the burrowing activity of Nereis virens and sediment nutrient flux, Mar. Ecol. Prog. Ser. 341 (2007) 111.
[22] E. Kristensen, Oxygen and inorganic nitrogen exchange in a Nereis virens(Polychaeta) bioturbated sediment-water system, J. Coast. Res. (1985) 109–116.
[23] L. Pischedda, J.-C. Poggiale, P. Cuny, F. Gilbert, Imaging oxygen distribution in marine sediments. The importance of bioturbation and sediment heterogeneity, Acta Biotheor. 56 (2008) 123–135.
[24] Q. Zhu, R.C. Aller, Y. Fan, Two-dimensional pH distributions and dynamics in bioturbated marine sediments, Geochim. Cosmochim. Acta 70 (2006) 4933–4949.
[25] E.D. Amato, S.L. Simpson, T.M. Remaili, D.A. Spadaro, C.V. Jarolimek, D.F. Jolley, Assessing the effects of bioturbation on metal bioavailability in contaminated sediments by diffusive gradients in thin films (DGT), Environ. Sci. Technol. 50 (2016) 3055–3064.
[26] USEPA, Portsmouth Naval Shipyard: Five-year Review Report, U.S. Environmental Protection Agency, Washingtong, DC, 2007.
[27] E. Kristensen, Impact of polychaetes (Nereis spp. and Arenicola marina) on carbon biogeochemistry in coastal marine sediments, Geochem. Trans. 2 (2001) 92–103.
[28] J.E. Winston, F.E. Anderson, Bioturbation of sediments in a northern temperate estuary, Mar. Geol. 10 (1971) 39–49.
[29] E. Michaud, G. Desrosiers, F. Mermillod-Blondin, B. Sundby, G. Stora, The functional group approach to bioturbation: the effects of biodiffusers and gallery-diffusers of the Macoma balthica community on sediment oxygen uptake, J. Exp. Mar. Biol. Ecol. 326 (2005) 77–88.
[30] F. Boano, J. Harvey, A. Marion, A. Packman, R. Revelli, L. Ridolfi, A. Wörman, Hyporheic flow and transport processes: mechanisms, models, and biogeochemical implications, Rev. Geophys. 52 (2014) 603–679.
[31] M.H. Garcia, Sediment transport and morphodynamics, in: Sedimentation Engineering: Processes, Measurements, Modeling, and Practice, 2008.
[32] J. Seeberg-Elverfeldt, M. Schlüter, T. Feseker, M. Kölling, Rhizon sampling of pore waters near the sediment/water interface of aquatic systems, Limnol. Oceanogr.: Methods 3 (2005) 361–371.
[33] G.R. Dickens, M. Koelling, D.C. Smith, L. Schnieders, Rhizon sampling of pore waters on scientific drilling expeditions: an example from the IODP expedition 302 Arctic Coring Expedition (ACEX), Sci. Drill. 4 (2007) 22–25.
[34] L. Shotbolt, Pore water sampling from lake and estuary sediments using Rhizon samplers, J. Paleolimnol. 44 (2010) 695–700.
[35] M. Xie, B.A. Jarrett, C. Da Silva-Cadoux, K.J. Fetters, G.A. Burton, J.-F. Gaillard, A.I. Packman, Coupled effects of hydrodynamics and biogeochemistry on Zn mobility and speciation in highly contaminated sediments, Environ. Sci. Technol. 49 (2015) 5346–5353.
[36] L.L. Stookey, Ferrozine—a new spectrophotometric reagent for iron, Anal. Chem. 42 (1970) 779–781.
[37] E. Viollier, P.W. Inglett, K. Hunter, A.N. Roychoudhury, P. Van Cappellen, The ferrozine method revisited: Fe (II)/Fe (III) determination in natural waters, Appl. Geochem. 15 (2000) 785–790.
[38] J.Y. Aller, R.C. Aller, Evidence for localized enhancement of biological associated with tube and burrow structures in deep-sea sediments at the HEEBLE site, western North Atlantic, Deep Sea Res. Part A Oceanogr. Res. Pap. 33 (1986) 755–790.
[39] G. Miron, G. Desrosiers, C. Retière, R. Lambert, Evolution spatio-temporelle du réseau de galeries chez le polychète Nereis virens (Sars) en relation avec la densité, Can. J. Zool. 69 (1991) 39–42.
[40] A. Piot, A. Rochon, G. Stora, G. Desrosiers, Experimental study on the influence of bioturbation performed by Nephtys caeca (Fabricius) and Nereis virens (Sars) annelidae on the distribution of dinoflagellate cysts in the sediment, J. Exp. Mar. Biol. Ecol. 359 (2008) 92–101.
[41] H. Stahl, K.W. Warnken, L. Sochaczewski, R.N. Glud, W. Davison, H. Zhang, A combined sensor for simultaneous high resolution 2-D imaging of oxygen and trace metals fluxes, Limnol. Oceanogr. Methods 10 (2012) 389–401.
[42] B.P. Boudreau, B. Jørgensen, Diagenesis and Sediment-Water Exchange, Oxford University Press, New York, 2001.
[43] B.L. O'Connor, M. Hondzo, Dissolved oxygen transfer to sediments by sweep and eject motions in aquatic environments, Limnol. Oceanogr. 53 (2008) 566–578.
[44] P.V. Ridd, Flow through animal burrows in mangrove creeks, Estuar. Coast. Shelf Sci. 43 (1996) 617–625.
[45] H.U. Riisgård, P.S. Larsen, Water pumping and analysis of flow in burrowing zoobenthos: an overview, Aquat. Ecol. 39 (2005) 237–258.
[46] J.W. Harvey, R.M. Chambers, J.R. Hoelscher, Preferential flow and segregation of porewater solutes in wetland sediment, Estuar. Coasts 18 (1995) 568–578.
[47] S. Heron, P. Ridd, The tidal flushing of multiple-loop animal burrows, Estuar. Coast. Shelf Sci. 78 (2008) 135–144.

[48] P.L. Shrestha, A.F. Blumberg, Cohesive sediment transport, in: M.L. Schwartz (Ed.), Encyclopedia of Coastal Science, Springer Netherlands, Dordrecht, 2005, pp. 327–330.
[49] K. Dyer, Coastal and Estuarine Sediment Dynamics, Wiley, Chichester, 1986.
[50] L. Thomsen, G. Gust, Sediment erosion thresholds and characteristics of resuspended aggregates on the western European continental margin, Deep Sea Res. Part I: Oceanogr. Res. Pap. 47 (2000) 1881–1897.
[51] E. De Deckere, T. Tolhurst, J. De Brouwer, Destabilization of cohesive intertidal sediments by infauna, Estuar. Coast. Shelf Sci. 53 (2001) 665–669.
[52] F. Orvain, P.-G. Sauriau, C. Bacher, M. Prineau, The influence of sediment cohesiveness on bioturbation effects due to Hydrobia ulvae on the initial erosion of intertidal sediments: a study combining flume and model approaches, J. Sea Res. 55 (2006) 54–73.
[53] J. Grant, G. Daborn, The effects of bioturbation on sediment transport on an intertidal mudflat, Neth. J. Sea Res. 32 (1994) 63–72.
[54] J. Yingst, D. Rhoads, Seafloor stability in central Long Island Sound: Part II. Biological interactions and their potential importance for seafloor erodibility, in: Estuarine Interactions, Academic Press, New York, 1978, pp. 245–260.
[55] A. Ciutat, J. Widdows, N.D. Pope, Effect of Cerastoderma edule density on near-bed hydrodynamics and stability of cohesive muddy sediments, J. Exp. Mar. Biol. Ecol. 346 (2007) 114–126.
[56] C. Soares, P. Sobral, Bioturbation and erodibility of sediments from the Tagus Estuary, J. Coast. Res. (2009) 1429–1433.
[57] B.L. O'Connor, J.W. Harvey, Scaling hyporheic exchange and its influence on biogeochemical reactions in aquatic ecosystems, Water Resour. Res. 44 (2008).
[58] J. Harvey, J. Drummond, R. Martin, L. McPhillips, A. Packman, D. Jerolmack, S. Stonedahl, A. Aubeneau, A. Sawyer, L. Larsen, Hydrogeomorphology of the hyporheic zone: stream solute and fine particle interactions with a dynamic streambed, J. Geophys. Res.: Biogeosci. (2005–2012) 117 (2012).
[59] J. Drummond, R. Davies-Colley, R. Stott, J. Sukias, J. Nagels, A. Sharp, A. Packman, Retention and remobilization dynamics of fine particles and microorganisms in pastoral streams, Water Res. 66 (2014) 459–472.
[60] D.J. Mayor, N.B. Gray, J. Elver-Evans, A.J. Midwood, B. Thornton, Metal-macrofauna interactions determine microbial community structure and function in copper contaminated sediments, PLoS One 8 (2013) e64940.

Interplay between Flow and Bioturbation Enhances Metal Efflux from Low-Permeability Sediments

Supporting Information

Minwei Xie [a,b,*], Ning Wang [a,c], Jean-François Gaillard [a], Aaron I. Packman [a]

[a] Department of Civil and Environmental Engineering, Northwestern University, 2145 Sheridan Road, Evanston, IL 60208-3109, USA

[b] Marine Environmental Laboratory, Shenzhen Research Institute, Hong Kong University of Science and Technology, Shenzhen 518000, China

[c] Faculty of Geosciences and Environmental Engineering, Southwest Jiaotong University, Chengdu, Sichuan, 610031, China

* Corresponding authors:

Minwei Xie, minwei.xie@gmail.com Tel: +86 0755 3355 2820 ; Fax: +86 0755 2267 3604

This supporting information consists of 23 pages, including 6 figures and 9 tables:

Table S1. Conditions for flume experiment.

Time	Duration	Shear stress (Pa)	Bioturbation
Day 0-28	4 weeks	0.11	No
Day 29-36	1 week	0.22	No
Day 36-42	1 week	0.11	No
Day 43-50	1 week	0.47	No
Day 51-57	1 week	0.11	No
4 hours on day 57	4 hours	0.58	No
Day 57-133	11 weeks	0.11	No
Day 134-148	2 weeks	0.11	Yes
Day 148-155	1 week	0.22	Yes
Day 155-162	1 week	0.11	Yes
Day 162-169	1 week	0.47	Yes
Day 169-176	1 week	0.11	Yes
4 hours on day 176	4 hours	0.58	Yes
Day 176-184	1 week	0.11	Yes

Table S2. Physicochemical properties of PNS sediments. Results are reported as mean values ± standard deviations from three replicate measurements. The sediments were characterized as described in our previous work [1].

Porosity (%)		41.2 ± 1.3
Permeability (m^2)		$1.7 \pm 0.5 \times 10^{-15}$
Grain Size Distribution	< 45 μm (%)	23
	45~106 μm (%)	17
	106~150 μm (%)	12
	150~250 μm (%)	6
	250~1000 μm (%)	16
	>1000 μm (%)	26
Total Cu (mg/kg dry sediment)		551 ± 49
Total Zn (mg/kg dry sediment)		510 ± 16
Total Fe (g/kg dry sediment)		21.6 ± 3.2

Cu and Fe analysis

Cu in water samples were measured using Zeeman Graphite Furnace Atomic Absorption Spectrometer (Z-GFAAS).[2] UV atomic absorbance of Cu was measured at 248.3 nm. NH_4NO_3 (5% v/v) (catalog no. 256064, Sigma Aldrich) was used as a chemical modifier to remove halide salts during the analysis. Standards were prepared by diluting Cu stock solution (1000 ppm, Sigma Aldrich) with NASS-4 open ocean reference seawater (National Research Council of Canada) to match the sample matrix. 20 µL sample with 20 µL modifier solution was co-injected into graphite cuvette for each analysis.

Fe (III) in water samples were determined with ferrozine colorimetric method [3]. Fe (III) in 1 mL of sample was first reduced to Fe (II) with 150 µL hydroxylamine hydrochloride solution (concentration, Sigma Aldrich) for 10 min. 200 µL ammonium acetate buffer solution (concentration, pH=9.5) (catalog number, Sigma Aldrich) and 100 µL ferrozine (concentration, Sigma Aldrich) were added and absorbance of the sample was measured at 562 nm with a UV-visible spectrophotometer (Spectronic 20, Spectronic Instrument).

Bed shear stress calculation

Stream velocity profiles obtained by Acoustic Doppler Velocimetry (ADV) were fit using the conventional logarithmic velocity profile for turbulent free-surface flow to determine the boundary shear stress.[3]

$$u(z) = \frac{u_*}{\kappa} \ln\left(\frac{z}{z_0}\right) = \frac{u_*}{\kappa} \ln(z) + b \qquad (S1)$$

where $u(z)$ is the longitudinal velocity at depth z above the SWI, z_0 is the roughness length, u_* is the shear velocity, κ is the Von Kármán constant (0.4), b is a constant. Nonlinear least squares fitting was use to fit equation (S1) to the longitudinal velocity data to obtain the shear velocity. Shear velocity was then converted to the shear stress using equation

$$\tau = \rho\, u_*^2 \qquad (S2)$$

where τ is the shear stress, and ρ is the density of the water in the flume experiments.

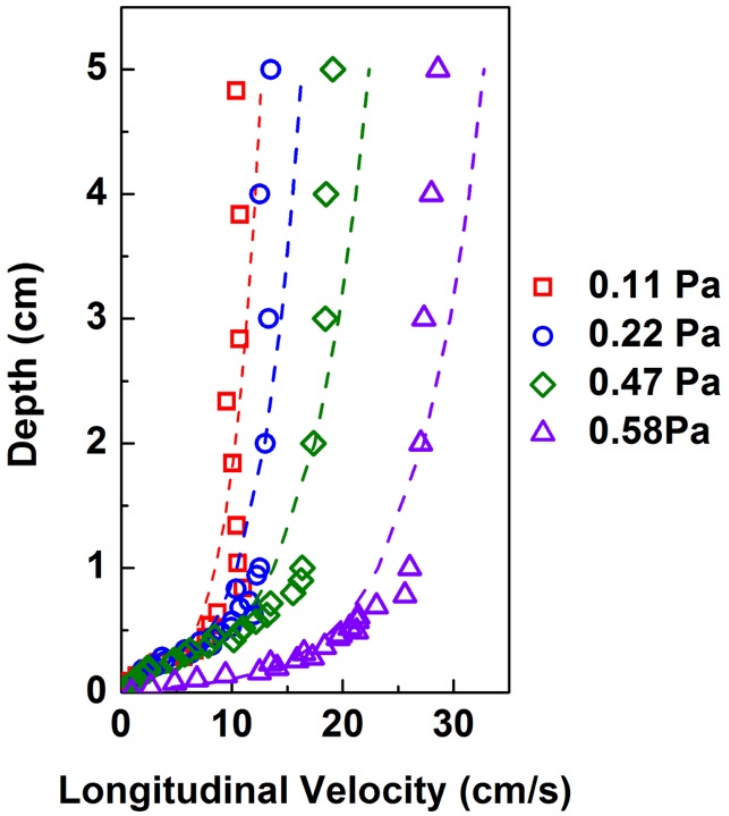

Figure S1. Free-stream velocity profiles measured in the water column by ADV and fit using Equation S1. The SWI is located at z = 0.

Evaluation of burrow openings and macroporosity

After introduction of 40 *Nereis virens*, 20 images of the entire bed surface were taken each day for two weeks. Burrows on each image were visually identified and independently counted with help of the multipoint tool in ImageJ. The total number of burrow openings in the entire bed surface was then calculated as the sum of openings in the 20 images. Temporal evolution of the total burrow openings is plotted in Figure S3.

An example image with a large number of burrows is shown in Figure S2a. The distribution statistics of burrow openings (mean area and standard deviation) were quantified in this example image and applied to all burrows detected in other images. In Figure S2a, each burrow opening was outlined by hand in Photoshop (Figure S2b), then binarized and converted into an areal distribution in ImageJ (Figure S2c,d). Observed burrow areas (mean ± standard deviation) were multiplied by the total number of surface openings determined above and normalized to the surface area of sediment bed to calculate the average macroporosity associated with burrows. Time-evolution of macroporosity is also plotted in Figure S3.

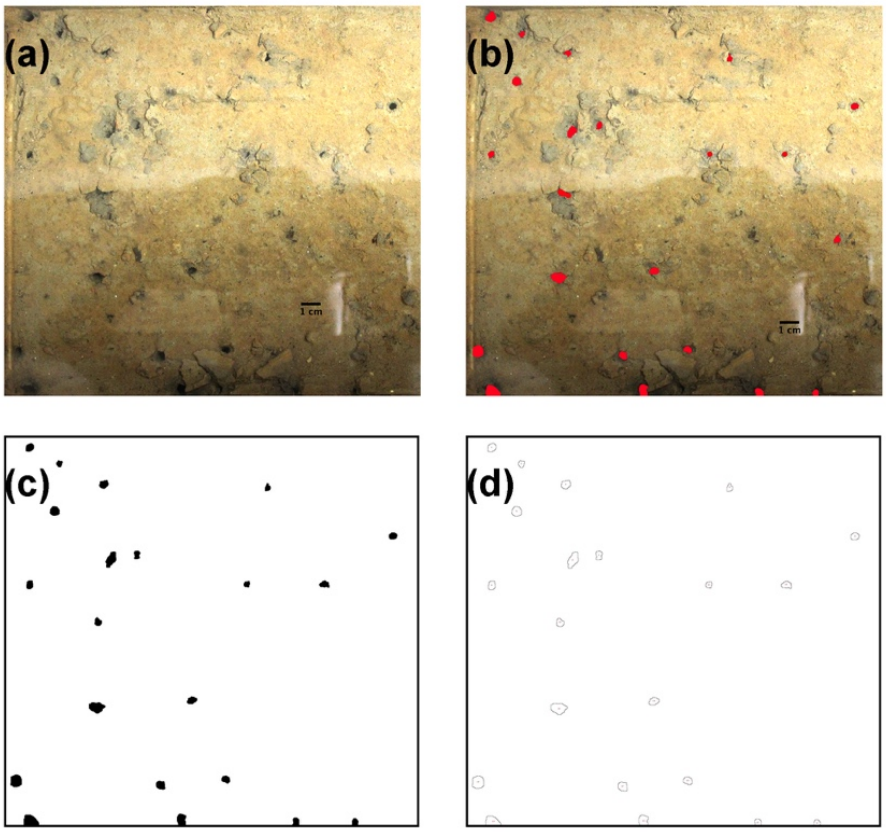

Figure S2. Determination of distribution statistics of burrow opening areas. (a) An example bed surface image with a large number of burrows. (b) The burrow openings were visually identified and outlined in Photoshop. (c) The image was then binarized in imageJ. (d) Area distribution of burrow openings were determined in ImageJ.

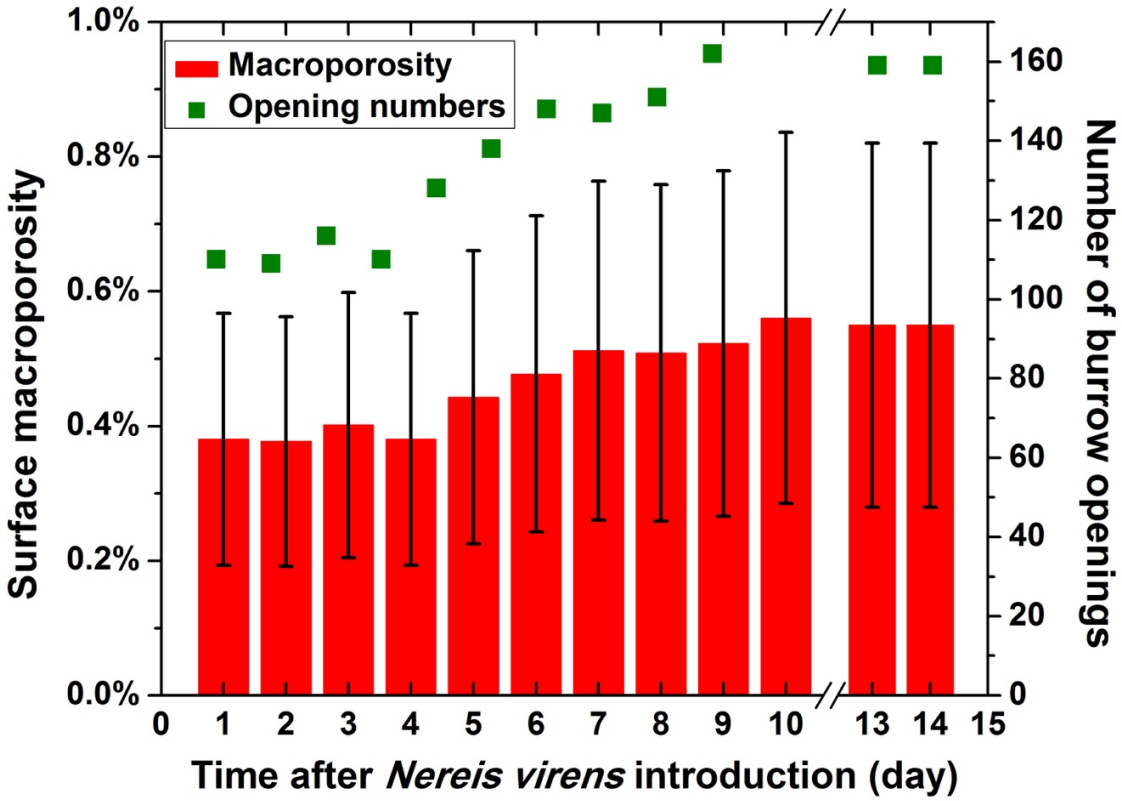

Figure S3. Development of worm burrow openings and surface macroporosity associated with *N. virens* burrows.

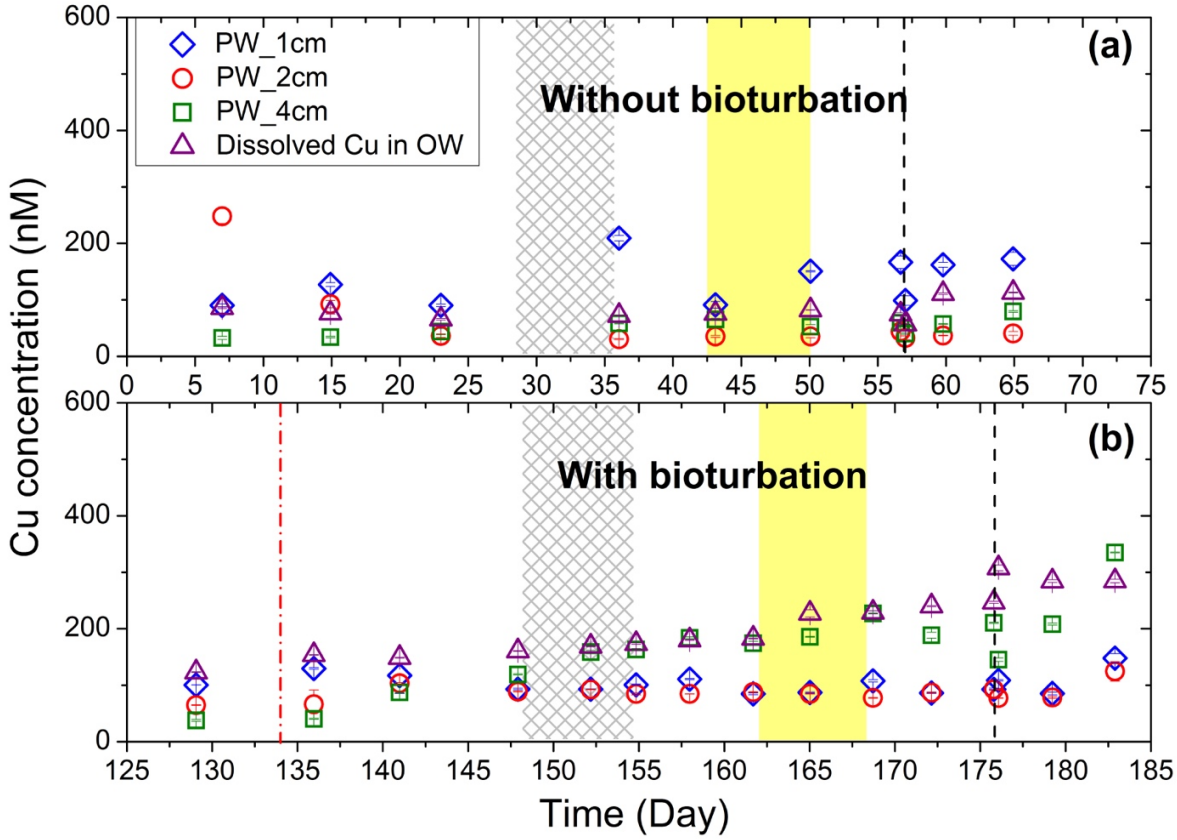

Figure S4. Temporal variations of Cu concentrations in porewater observed by RISS emplaced at different depths (a) Without bioturbation, (b) With bioturbation. Porewater samples were collected from RISS located at x = 0.9 m. Unshaded areas of the graphs indicate periods with baseline shear conditions (0.11 Pa). Cross-hatching and shading indicate periods with shear stresses of 0.22 Pa and 0.47 Pa, respectively. Black vertical dashed lines in day 57 (a) and day 176 (b) represent 4-hour resuspension events. Red vertical dashed line on day 134 (b) represents introduction of 40 *N. virens*.

Dissolved oxygen profiles.

At the end of each period of constant flow (0.11, 0.22, 0.47 and 0.58 Pa), DO concentrations in porewater were measured *in situ* using an oxygen microelectrode (OX-100, Unisense, Denmark). Oxygen measurements were performed in locations with intact sediments, i.e., avoiding burrow openings. The microelectrode was mounted on a microprofiler with computerized depth control and driven vertically into the sediment bed with a step size of 125 μm. Two replicate DO profiles were measured for each flow condition, with the exception of sediment resuspension conditions, for which only one DO profile was measured owing to the short duration of the resuspension event.

Penetration of oxygen into the sediment is controlled by the dynamic balance between transport of oxygen from overlying water and consumption within the sediment bed [4]. DO concentrations were maintained at a constant level in the overlying water owing to rapid transfer from the atmosphere, but decreased rapidly within the sediment bed (Figure S5). The O_2 penetration depth (OPD) was defined as the depth at which the porewater oxygen concentration dropped to 1% of the overlying water oxygen concentration. Before introduction of *N. virens*, OPDs were 1.500, 1.850, 3.200, and 4.125 mm at shear stresses of 0.11, 0.22, 0.47, and 0.58 Pa, respectively (Figure S5a). The strong correlation between OPD and flow shear ($r=0.99$, $p<0.01$) indicates that hydrodynamic forcing enhanced O_2 penetration into the sediments. Following reduction of flow shear from 0.58 to 0.11 Pa on day 57, OPD decreased to 2.500 mm on day 64 (Figure S5b). After *N. virens* was introduced into the sediments, OPDs increased to 4.125, 5.000, 4.750, and 5.875 mm at shear stresses of 0.11, 0.22, 0.47, and 0.58 Pa, respectively (Figure S5b). All of these OPDs are much greater than the OPD under baseline shear (0.11 Pa) before

introduction of *N. virens* (2.500 mm), indicating that interactions between flow and bioturbation enhanced the penetration of oxygen into sediments (Figure S5b).

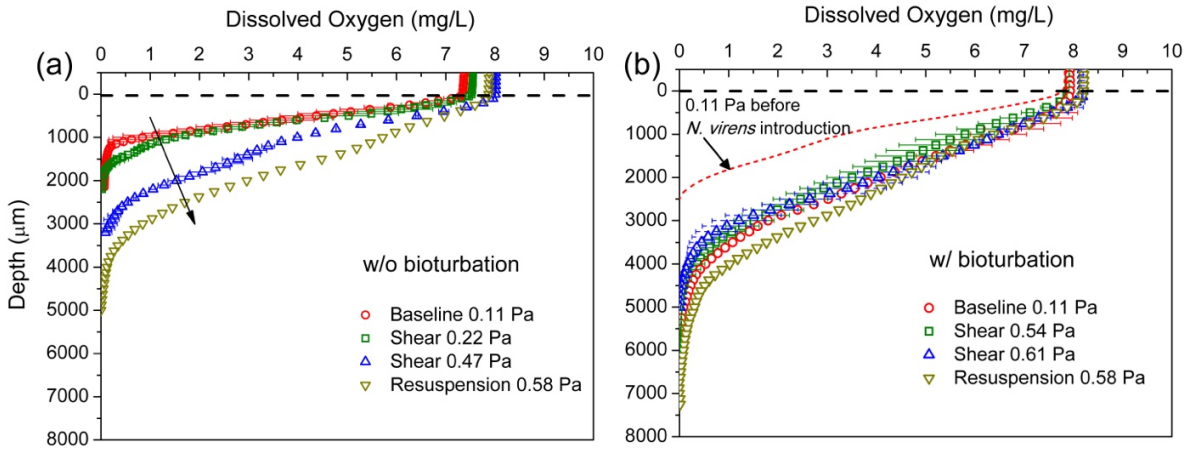

Figure S5. Dissolved oxygen profiles under varied hydrodynamic conditions without (a) and with (b) bioturbation. Oxygen profiles for shear stresses of 0.11, 0.22 and 0.47 Pa represent an average of two replicate measurements, and error bars represent the standard deviation. Only 1 profile was obtained under the resuspension condition, 0.58 Pa (yellow triangles). Red dashed curve in (b) represent DO profile measured under baseline shear (0.11 Pa) without bioturbation in day 64, one week after the first sediment resuspension in day 57. Black horizontal dashed lines represent the sediment water interface.

Statistical analysis for Cu concentrations in porewaters and corresponding overlying water samples

Statistical analyses are based on student's t test. The Cu concentrations in porewater at different depths and Cu concentrations in the overlying water collected at the same time were cross compared (Table S3~S8). The null hypothesis states no difference between the compared two groups and a p value < 0.05 suggests the two groups are statistically different from each other. Statistical analyses were performed independently to the datasets before and after introduction of *N. virens* on day 134.

Results for Cu concentrations in porewater collected at x = 1.2 m before and introduction of *N. virens* are shown in Table S3 and S4, and indicated that Cu concentrations at different depths as well as in the overlying water were significantly different from each other with and without bioturbation.

Results for Cu concentrations in porewater collected at x = 0.9 m before and introduction of *N. virens* are shown in Table S5 and S6, and also indicated that Cu concentrations at different depths as well as in the overlying water were significantly different from each other with and without bioturbation.

Cu concentrations in porewater at different depths collected at x = 1.2 m were also compared with Cu concentrations in porewater at corresponding depths collected at x = 0.9 m before and after the introduction of *N. virens* (Table S7, S8). Results showed that before introduction of *N. virens*, the Cu concentrations in porewater at corresponding depths collected at different locations were similar (Table S7), indicating good reproducibility of porewater Cu concentrations along the flume. However, after the introduction of *N. virens* on day 134, the Cu concentrations in porewater at corresponding depths collected at different locations became

significantly different (Table S8), suggesting bioturbation caused heterogeneity in porewater metal chemistry.

Table S3. Statistical results of Cu concentrations in porewater at x = 1.2 m and corresponding Cu concentrations in overlying water before introduction of *Nereis virens* on day 134. Statistic results indicated that before introduction of *Nereis virens,* dissolved Cu concentrations measured at 1 cm porewater were significantly higher than those measured in overlying water and in porewater at depth > 1 cm.

	PW_1 cm	PW_2 cm	PW_4 cm	OW
PW_1 cm				
PW_2 cm	p <0.001			
PW_4 cm	p <0.001	p <0.001		
OW	p <0.005	p <0.005	p <0.005	
$[Cu]_d$ (nM)	163 ± 57	67.6 ± 26.9	52.8 ± 13.1	91.5 ± 25.0

Table S4. Statistical results of Cu concentrations in porewater at x = 1.2 m and corresponding Cu concentrations in overlying water after introduction of *Nereis virens* on day 134. Statistic results indicated that after introduction of *Nereis virens,* dissolved Cu concentrations measured at 2 cm porewater were significantly higher than those measured in overlying water and in porewater at other depths.

	PW_1 cm	PW_2 cm	PW_4 cm	OW
PW_1 cm				
PW_2 cm	p < 0.001			
PW_4 cm	p < 0.001	p < 0.001		
OW	p < 0.05	p < 0.005	p < 0.001	
$[Cu]_d$ (nM)	188 ± 32	463 ± 189	55.3 ± 20.2	213 ± 54

Table S5. Statistical results of Cu concentrations in porewater at x = 0.9 m and corresponding Cu concentrations in overlying water before introduction of *Nereis virens* on day 134. Statistic results indicated that before introduction of *Nereis virens,* dissolved Cu concentrations measured at 1 cm porewater were significantly higher than those measured in overlying water and in porewater at depth > 1 cm.

	PW_1 cm	PW_2 cm	PW_4 cm	OW
PW_1 cm				
PW_2 cm	p <0.001			
PW_4 cm	p <0.001	p <0.001		
OW	p <0.005	p <0.005	p <0.005	
$[Cu]_d$ (nM)	135 ± 42	64.7 ± 58.6	49.6 ± 13.8	91.5 ± 25.0

Table S6. Statistical results of Cu concentrations in porewater at x = 0.9 m and corresponding Cu concentrations in overlying water after introduction of *Nereis virens* on day 134. Statistic results indicated that after introduction of *Nereis virens,* dissolved Cu concentrations measured at 4 cm porewater were significantly higher than those measured in overlying water and in porewater at other depths.

	PW_1 cm	PW_2 cm	PW_4 cm	OW
PW_1 cm				
PW_2 cm	p < 0.001			
PW_4 cm	p < 0.001	p < 0.001		
OW	p < 0.05	p < 0.005	p < 0.001	
$[Cu]_d$ (nM)	103 ± 19	87.8 ± 13.7	173 ± 69	213 ± 54

Table S7. Statistical results of Cu concentrations in porewater collected at x = 0.9 and 1.2 m before introduction of *Nereis virens* on day 134. Statistical results indicated that before introduction of *Nereis virens,* Cu concentrations in porewater at different depths measured at x = 0.9 m were similar to those measured at x = 1.2 m.

		RISS at x = 0.9 m		
		PW_1 cm	PW_2 cm	PW_4 cm
RISS at x = 1.2 m	PW_1 cm	p = 0.15		
	PW_2 cm		p = 0.88	
	PW_4 cm			p = 0.47

Table S8. Statistical results of Cu concentrations in porewater collected at x = 0.9 and 1.2 m after introduction of *Nereis virens* on day 134. Statistical results indicated that after introduction of *Nereis virens,* Cu concentrations in porewater at different depths measured at x = 0.9 m were significantly different from those measured at x = 1.2 m.

		RISS at x = 0.9 m		
		PW_1 cm	PW_2 cm	PW_4 cm
RISS at x = 1.2 m	PW_1 cm	p <0.001		
	PW_2 cm		p < 0.001	
	PW_4 cm			p < 0.001

Determination of net flux and statistical analyses

The rate of change in dissolved Cu concentrations in the overlying water was first determined by linear least-squares fitting of the dissolved Cu concentrations (Figure S6). Net flux in each hydrodynamic conditions was then obtained by normalizing the changing rates to the volume of recirculating overlying water and the surface area of sediment bed. As Cu release at shear 0.47 and 0.58 Pa with bioturbation (Figure S6 g,h) were rapid, which were distinct from those in other conditions, only two data points before and after the change of hydrodynamic conditions were used to calculate the instantaneous fluxes.

Since the net fluxes were calculated from the changing rate of dissolved Cu concentrations, which were the slope coefficients of the regressed lines, statistical analyses (ANCOVA) were performed by comparing the slopes of regression lines using software Minitab 17 and results are summarized in Table S9. The underlying mechanism of conducting a student's t test is reported in Andrade et al.[5] As only two points were used in conditions of 0.47 and 0.58 Pa shear with bioturbation, statistical analyses were not performed on these two conditions.

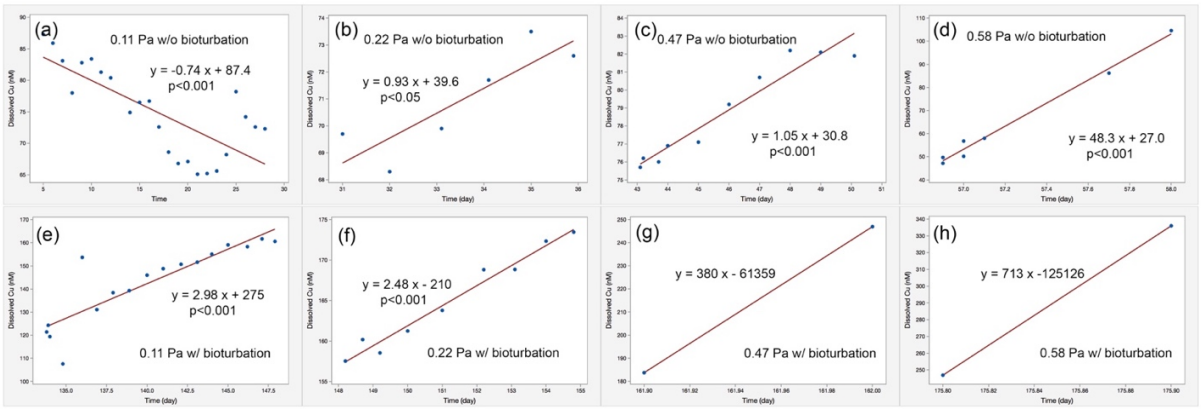

Figure S6. Regressions of dissolved Cu concentrations in the overlying water under varying conditions.

Table S9. Summary of statistical results from linear regressions of Cu concentrations in overlying water under different conditions.

	0.11 Pa w/o	0.22 Pa w/o	0.47 Pa w/o	0.58 Pa w/o	0.11 Pa w/	0.22 Pa w/
0.11 Pa w/o						
0.22 Pa w/o	p=0.126					
0.47 Pa w/o	p<0.005	p=0.652				
0.58 Pa w/o	p<0.001	p<0.001	p<0.001			
0.11 Pa w/	p<0.001	N.A.	N.A.	N.A.		
0.22 Pa w/	N.A.	p<0.001	N.A.	N.A.	P=0.642	

w/o represents "without bioturbation"
w/ represents "with bioturbation"
N.A. represents "Not Analyzed"

References:

[1] M. Xie, N. Wang, J.-F. Gaillard, A.I. Packman, Hydrodynamic Forcing Mobilizes Cu in Low-permeability Estuarine Sediments, Environmental Science & Technology, 50 (2016) 4615-4623.

[2] M. Taillefert, The distribution of trace elements cobalt and lead at the oxic-anoxic transition of a stratified lake : analytical speciation and modeling, in, Thesis (Ph.D., Civil Engineering)--Northwestern University, 1997.

[3] E. Viollier, P.W. Inglett, K. Hunter, A.N. Roychoudhury, P. Van Cappellen, The ferrozine method revisited: Fe (II)/Fe (III) determination in natural waters, Applied Geochemistry, 15 (2000) 785-790.

[4] W. Ziebis, S. Forster, M. Huettel, B.B. Jørgensen, Complex burrows of the mud shrimp Callianassa truncata and their geochemical impact in the sea bed, Nature, 382 (1996) 619-622.

[5] J. Andrade, M. Estévez-Pérez, Statistical comparison of the slopes of two regression lines: a tutorial, Analytica chimica acta, 838 (2014) 1-12.